FINAL DESIGN REPORT

AER406 – AIRCRAFT DESIGN
Borren Moe – 1000988489 Mitchell Passarelli – 999845896
Thomas Ulph – 999640321 Carrie Ran Yan – 999888126

Table of Contents

List of Tables

List of Figures

List of Symbols

Symbol	Meaning
AoA, α	Angle of attack
AR	Aspect ratio
BLF	Buckling load factor
BWB	Blended wing-body
b	Wingspan
CAD	Computer-aided design
C_D	Drag coefficient
CFD	Computational Fluid Dynamics
CG	Centre of gravity
C_L	Lift coefficient
$C_{L\alpha}$	Lift curve slope (with respect to angle of attack)
$C_{L\delta}$	Lift curve slope with respect to elevon deflection
C_M	Moment coefficient
$C_{M\alpha}$	Moment curve slope (with respect to angle of attack)
$C_{M\delta}$	Moment coefficient slope with respect to elevon deflection
D	Drag force
EW	Empty weight (mass)
FEA	Finite Element Analysis
FOS	Factor of safety
g	Acceleration due to gravity (9.81 m/s^2)
L	Lift force
LE	Leading edge
M	Aerodynamic moment
MAC	Mean aerodynamic chord
m	Total aircraft mass
n	Load factor
PPB	Payload prediction bonus
RPM	Revolutions per minute
r_c	Turn radius
S	Planform area
s_g	Ground roll/take-off distance
T	Thrust
TE	Trailing edge
t	Flight course time
v	Speed
v_{hw}	Headwind speed
v_{LO}	Liftoff speed
W	Weight (force)
x_{CG}	Chordwise location of the center of gravity
x_{NP}	Chordwise location of the neutral point
δ_e	Elevon deflection angle
μ_r	Coefficient of rolling friction
ϕ	Turning bank angle
ω_c	Turn rate

1 Design Overview

1.1 Score Breakdown & Cost Function Analysis

Table 1 below provides a high-level score breakdown and the estimate of the total flight score.

Table 1 - Score Breakdown

Score Component	Value	Comments
CU	1,010	8 tennis balls, 5 ping pong balls, 0 golf balls
PF	0.378	Total mass ≈ 1.3 kg, payload mass ≈ 0.5 kg
f(t)	1.27	Average speed = 15 m/s, bank angle = 70°
TB	1.25	Headwind ≥ 2 m/s, landing gear slope = 5°
STB	1.2	Full static and dynamic stability
CB	2	BWB configuration
PPB	???	TBD
VB	250	
Total	**1,710**	**Excludes PPB**

These estimates stem from the following requirements for the aircraft:

1. The aircraft shall carry a minimum payload of 100 CU
    a. The aircraft should carry a payload that maximizes the combined multiplier PFxCU.
2. The aircraft shall be capable of taking off within 20 ft.
    a. The aircraft should minimize structural mass.
3. The aircraft shall be designed to minimize the flight time around the course.
    a. The aircraft should maximize the flight time scoring bonus as a fast flyer.
4. The aircraft shall be passively stable for 8 seconds without control input.
5. The aircraft shall be a blended wing body configuration, according to the following definitions:
    a. The transition from body chord to wing chord shall occur before 50% of the total half span.
    b. The wing chord shall be at least a 30% reduction of the body chord length over a small span.
6. The aircraft shall fly at a minimum 30° bank angle during the turns in the course.
7. The aircraft shall carry the required electronic components (detailed in Table 2).
8. The aircraft shall be capable of capturing images of a target using the video camera.

1.2 Aircraft CAD Model

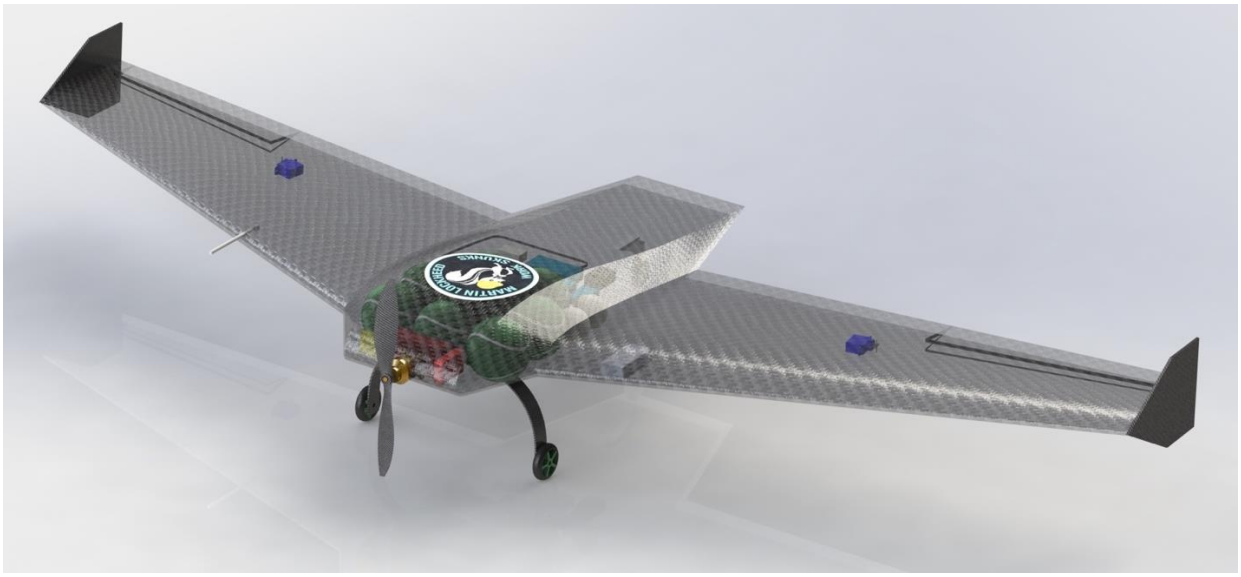

Figure 1 - Aircraft CAD Model

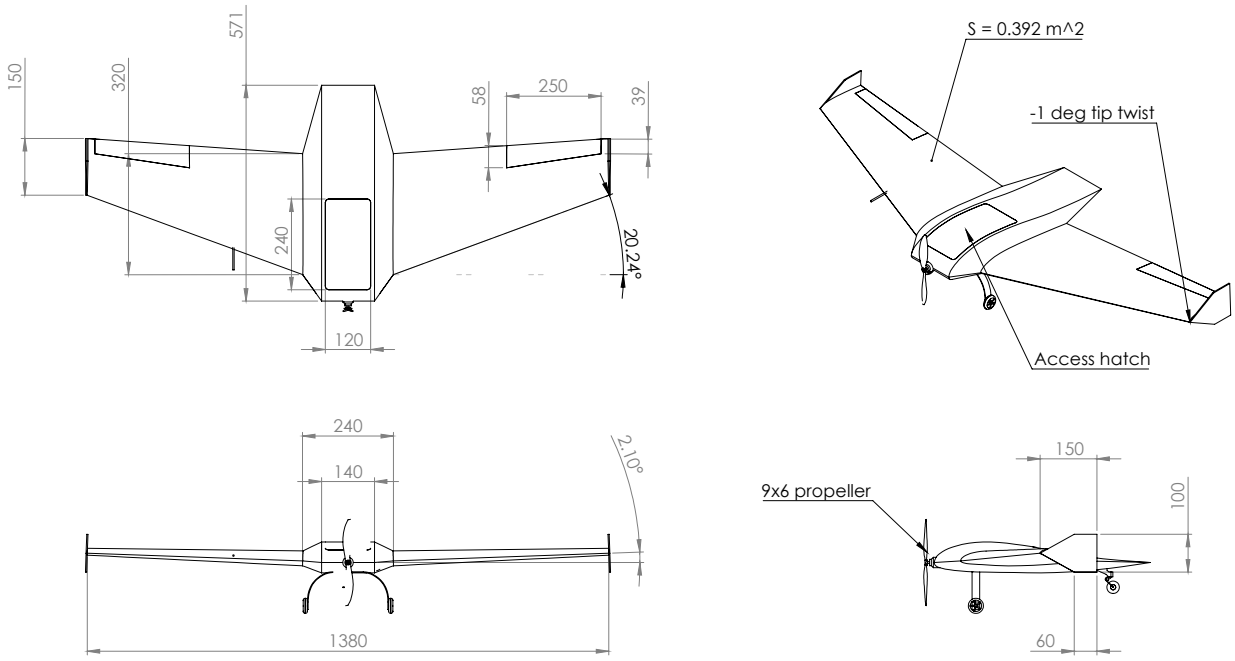

Figure 2 - Aircraft Planform Drawing (dimensions in mm)

1.3 Component & Payload Layout

Cargo loading is an important factor in determining flight score and overall aircraft performance parameters such as take-off distance and maximum cruise speed. The fully loaded configuration will consist of 8 tennis balls, 5 ping-pong balls and no golf balls. The position of the cargo plays an important role in the stability of the aircraft. To ensure static pitch stability and have sufficient static margin, the

center of gravity is designed to be 141 mm from the leading edge using the payload and component layout in Figure 4. Tennis balls are heavier than ping-pong balls and therefore are placed as forward as possible. The lighter ping-pong balls are placed aft in whatever space left available.

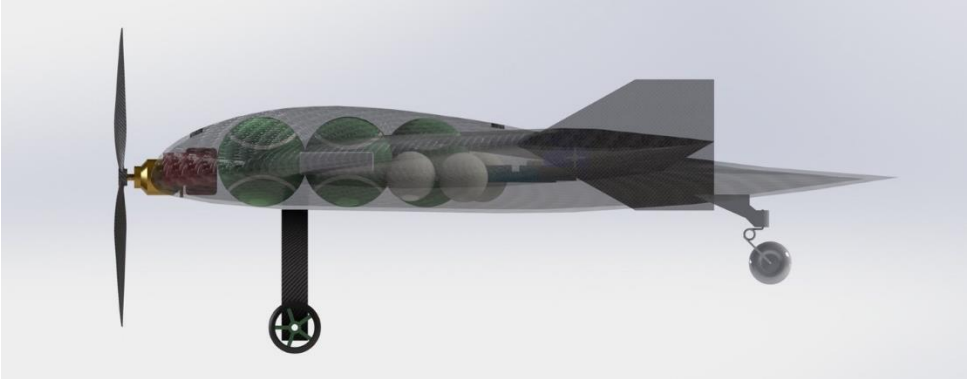

Figure 3 - Aircraft Profile

In addition to the cargo, other key components must be fit to the aircraft. The aircraft shall carry a battery, a BDC motor, an ESC, a buzzer, a camera, a Pitot tube, a signal receiver, two servo motors, as well as measurement IMU and GPS. Basing on the same consideration made for the cargo, heavier electronics such as the battery, the ESC, the buzzer and the motor are placed in the front of the aircraft. The lighter components such as the GPS, IMU and eLogger are placed aft of the cargo in order to shift cargo as forward as possible. Servo motors are placed near the control surfaces. The Pitot tube and the camera are placed on either side of the wing to balance out the weight. The Pitot tube is placed far enough to the side to stay out of the prop-wash.

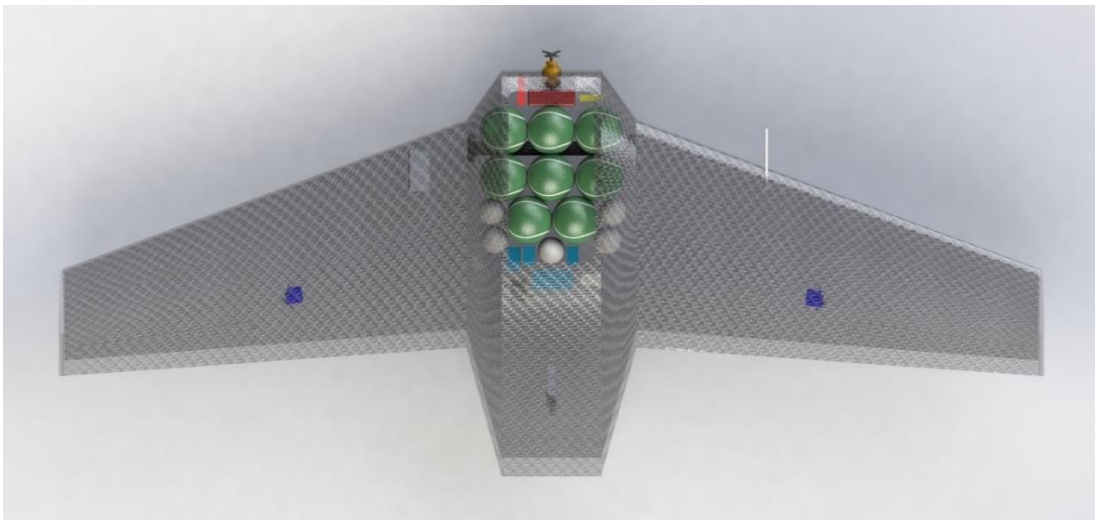

Figure 4 - Aircraft Interior Layout

Cables run through the middle of the aircraft to connect everything together. The detailed layout of the wiring is shown in Figure 5 below. The battery and ESC, DC motor and buzzer are placed in the front of the aircraft. A cable will need to run down the center of the fuselage where the receiver is and power will need to be supplied to the sensors and receiver.

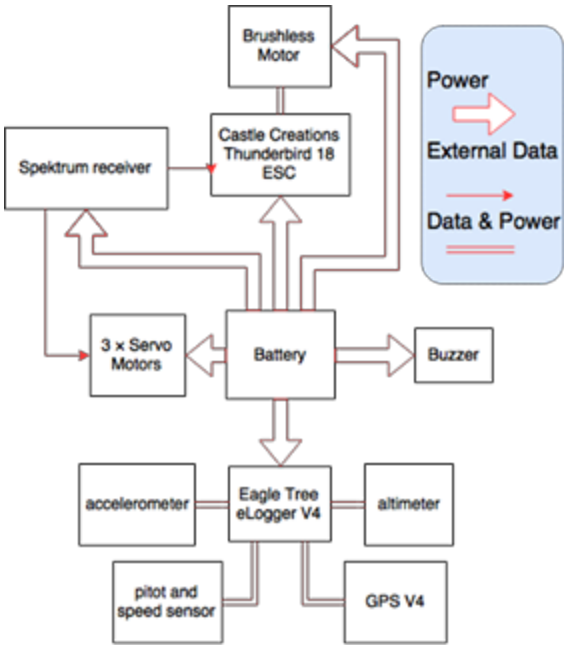

Figure 5 - Electronic Component Layout Diagram

1.4 Mass Budget

Mass is a critical consideration in aircraft design process. The goal is to reduce the weight of the aircraft as much as possible in order to optimize payload fraction score, while maximizing the payload it can carry. Certain components of the aircraft are provided, and thus considered as fixed components. These includes the sensors, receiver, battery, and motors. The structure, along with landing gear, propellers, and control surfaces account for another portion of the total weight. Lastly, the payload will be considered towards the total weight. A detailed breakdown is shown in Table 2 below.

Table 2 - Mass Budget

Item	Mass (g)
Fixed Components:	
Spektrum Receiver	9
AXI -2217/16 Gold-Line Motor	80.5
Castle Creations Thunderbird 18 ESC	25.5
Eagle Tree eLogger V4	21
Eagle Tree 3 axis Accelerometer	4.3
Eagle Tree Altimeter	4.1
Eagle Tree GPS V4	16.5
Eagle Tree Pitot Tube / Speed Sensor	13
Battery Buzzer	5
Variable Components:	

ElectriFly 1300mAh 30C 11.1V Battery	110.5
E-flite EF 721 HD Camera	14
HiTec HS-55 Servos	18
Propeller 9x6 (carbon fiber pre-fabricated)	16
Landing Gear	40
Airframe Mass (See Appendix 7D)	462.2
Payload:	
Ping Pong Balls	13.5
Tennis Balls	470.4
Total Mass	1323.5

The total empty mass of the aircraft frame and all essential components is 839.6 g with the aircraft body massing 462.2 g. The airframe mass is estimated based on a total surface area of 0.818 m^2 and has a margin of 10% to account for excess epoxy and joint layers during manually manufacturing. The expected full payload is 483.9 g, which consists of 8 tennis balls and 5 ping-pong balls, making the total aircraft gross mass 1323.5 g. At full load, 37% of the total mass will be from payload.

2 Aerodynamics

Our configuration is a Blended Wing Body (BWB). The approach used in designing the aerodynamic shape of the aircraft was to divide the planform into body, wing and transition sections. Airfoils were then selected for the body and wing sections based on a range of predicted Reynolds numbers. The following subsections provide in-depth analyses of the airfoil selection and planform design processes.

2.1 Airfoil Selection

2.1.1 Background Survey

A survey of past designs provided set of airfoils that were commonly used for flying wings or BWB aircraft. A joint paper from Cambridge University and MIT [1] stated that due to the lack of a tail for a BWB configuration, airfoils with reflex are required to elicit a nose up pitching moment. Alternatively, it is possible to correct typical airfoil pitching moments with extensive wing sweep and twist, but this causes an induced drag penalty and increased wing design complexity. For these reasons, preference will be given to airfoils with reflex.

A master's thesis from RMIT University highlighted the Quabeck, Eppler and DAE series of airfoils as potential candidates for BWB aircraft due to high thickness-to-chord ratio that permit the storage of high-volume payloads [2]. The thesis suggests MH45 and MH60 airfoils for use with flying wings, which also can be applied for use on BWB aircraft. These airfoils will serve as a benchmark for comparison with any additional airfoils that are found.

2.1.2 Selection Criteria

Airfoil selection was broken into two main categories: body airfoils, where the payload would be stored, and wing airfoils which would serve to primarily generate lift. Since the ability to carry payload directly increased the score function, selection of the body airfoils occurred first.

- Airfoil Thickness: In a Boeing research paper, it was suggested that airfoils with a thickness of 17% should be taken as a maximum [3]. Higher values begin to result in adverse aerodynamic effects and lower values reduce payload volume for a given chord length. A shorter chord is preferred as there is less viscous drag due to a smaller surface area and the pitching moment is less influential due to a shorter moment arm. A lower bound of 5% was set on wing airfoil thickness to permit simpler fabrication.
- C_L versus α: aircraft mass is a main driver as it directly affects payload fraction score multiplier, thus a lighter aircraft is best. With a higher C_L, less surface area is required, which in turn requires less structural mass. An ideal airfoil candidate should attempt to maximize C_L.
- C_D versus α: as evidenced by analysis of the time scoring function, a faster aircraft will yield a higher score. This results in a selective pressure that favors airfoils with a relatively low C_D over the operational angles of attack.
- C_M versus α: as mentioned before, reflex airfoils are desired due to the positive pitching moment required for aircraft stability.
- Reynolds Number: the BWB aircraft will be operating at slow speeds (15 m/s) with a short chord length, thus the Reynolds number will be relatively low, on the order of 100,000 (for the wing airfoil) to 500,000 (for the body airfoil). Airfoils should have “well-behaved” characteristic in this Re range and if possible, promote laminar flow by maintaining a favorable pressure distribution.

Airfoil Tools [4] was used to search the UIUC airfoil database. Initially, highly cambered airfoils with a high CL were considered for the wing airfoils, such as the DAE series and low number Eppler series. However, it quickly became apparent that airfoils with a high C_L were associated with a highly negative pitching moment. As a result, it was decided that a C_L penalty would be accepted to permit a more positive pitching moment for better stability. The following figures show a comparison between a number of body and wing airfoils.

2.1.3 Selected Airfoils

2.1.3.1 Body Airfoil

A Fauvel 14% airfoil was selected for the main body of the aircraft. Figure 6 shows a comparison of the C_M – α plot for a number of candidate airfoils, note how C_M remains relatively high over the operational α range. In Figure 7, it can be seen that the Fauvel has a lower $C_{L,max}$, however, this performance decrease is accepted as a trade for a higher positive pitching moment.

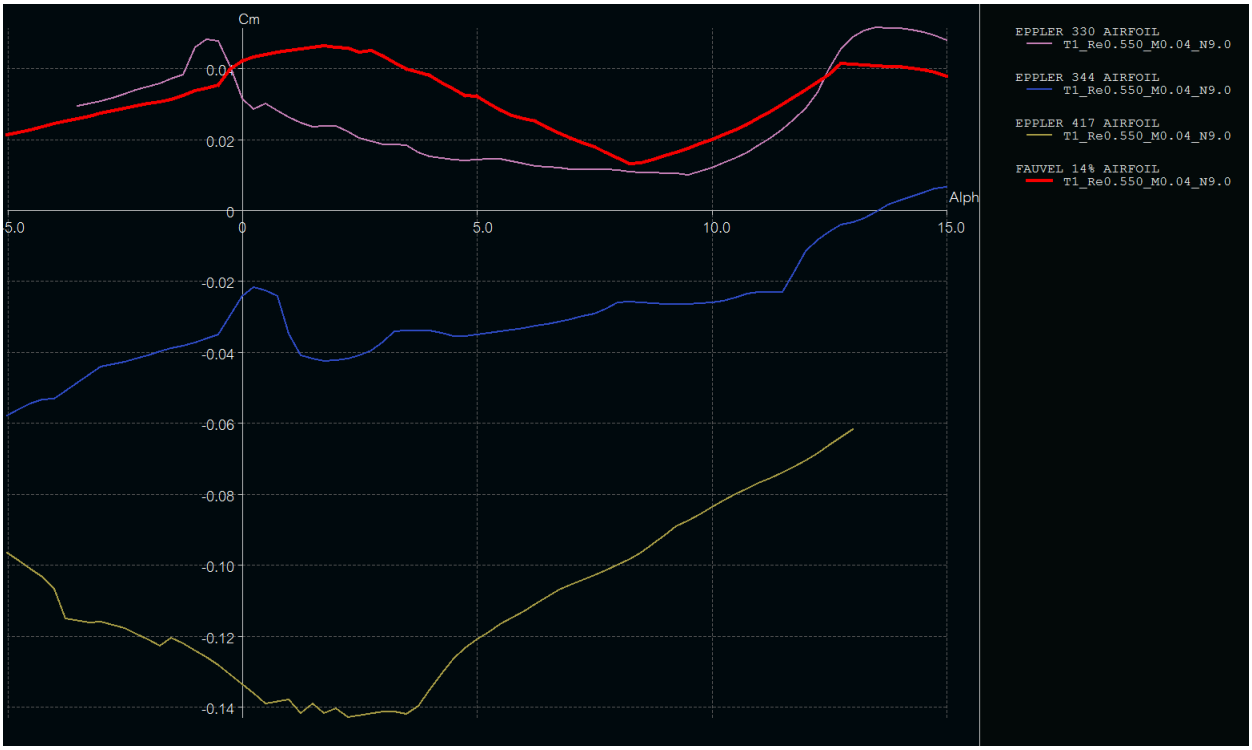

Figure 6 - Pitching Moment XFLR5 Plot for Various Body Airfoils (Selected Airfoil in Red)

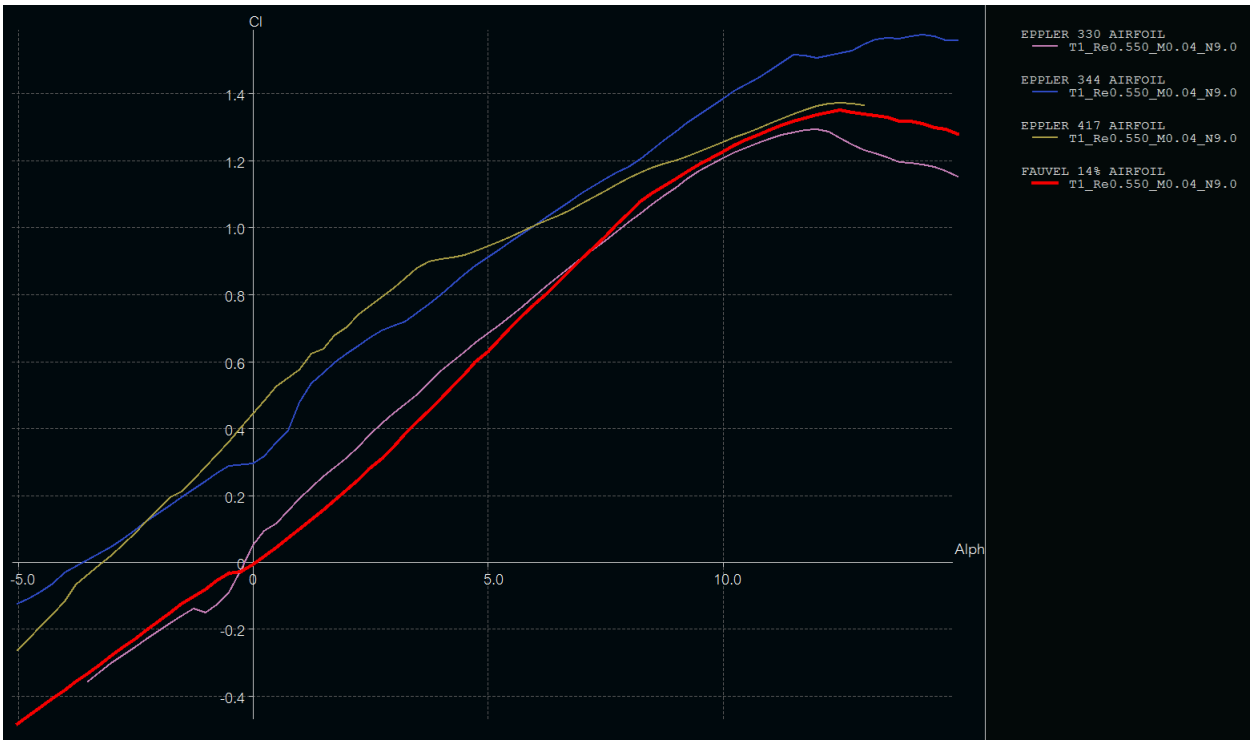

Figure 7 - Lift Coefficient XFLR5 Plot for Various Body Airfoils (Selected Airfoil in Red)

Fauvel 14% Specifications:

- See Figure 8 for airfoil profile.
- $C_{L,max}$ of 1.35 occurs at an α of 12.5° and the lift slope remains relatively linear.
- The pitching moment is entirely positive, ranging from 0.013 to 0.046.
- The drag coefficient remains low and reasonably constant from 0.008 to 0.02 over the operational α.
- Stall occurs at about 13°, this value from XFLR5 was agreable to experimental data found.
- Max C_L/C_D is 94 which occurs before stall at 9°.
- A chord length of 571 mm was selected to allow longitudinal placement of 3 tennis balls.

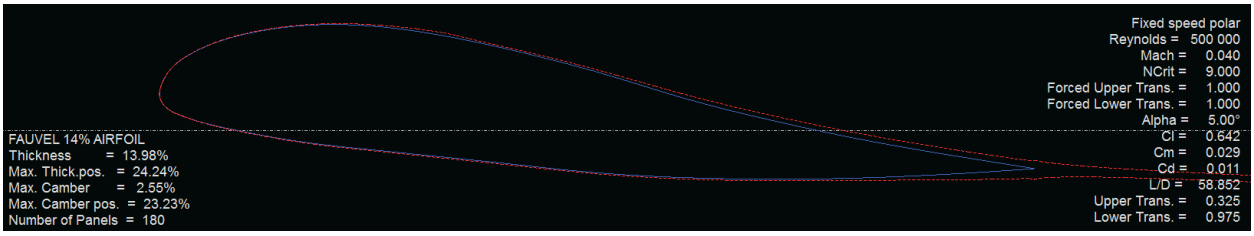

Figure 8 - Fauvel 14% Airfoil Profile at 5°

2.1.3.2 Wing Airfoil

When compared to other candidate airfoils, the NACA 24112 has a higher pitching moment, as seen in Figure 9, permitting the aircraft to be statically stable. Once again, due to the positive pitching moment, it suffers from a low $C_{L,max}$ when compared to airfoils such as the DAE-51, shown in Figure 10.

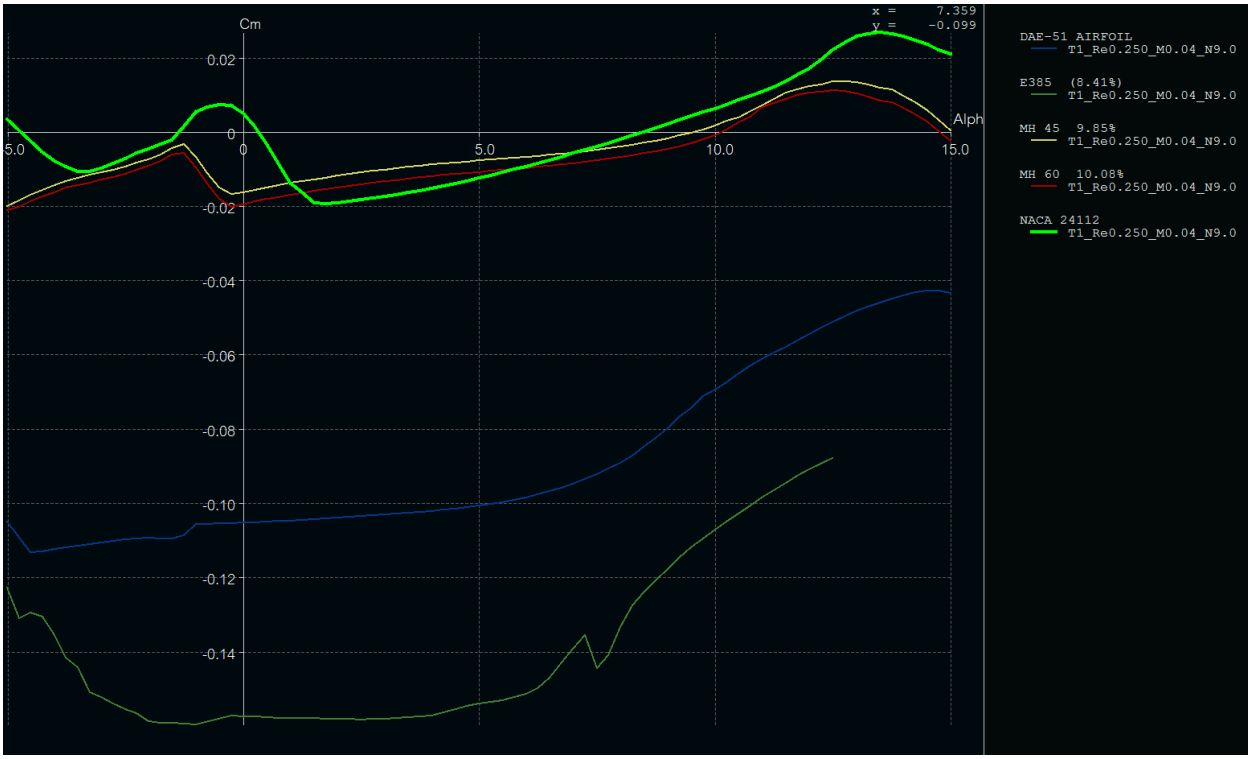

Figure 9 - Pitching Moment XFLR5 Plot for Various Wing Airfoils (Selected Airfoil in Green)

Figure 10 - Lift Coefficient XFLR5 Plot for Various Wing Airfoils (Selected Airfoil in Green)

NACA 24112 Specifications Figure:

- See Figure 11 for airfoil profile.
- $C_{L,max}$ of 1.3 occurs at an α of 13° and the lift slope remains relatively linear.
- The pitching moment is close to zero and ranges between -0.02 to 0.026.
- The drag coefficient is slightly higher than the Fauvel and is between 0.01 to 0.02 over the operational α.
- Stall occurs at about 13°, which was confirmed by experimental data.
- Max C_L/C_D is 63.5 which occurs at 10°.
- A chord minimum cord length was selected to be 150 mm to allow for easier fabrication.

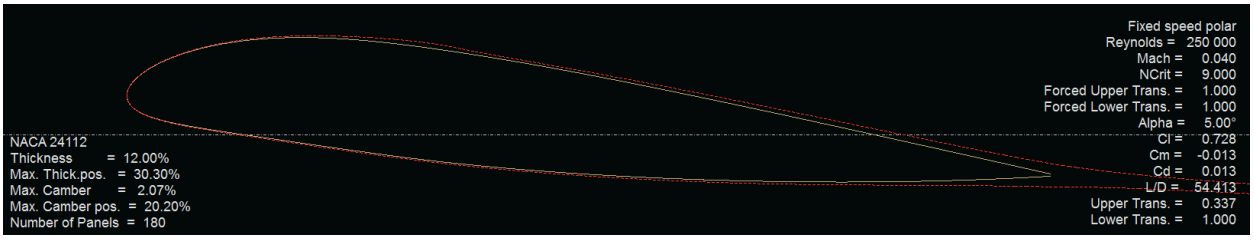

Figure 11 - NACA 24112 Airfoil Profile at 5°

2.2 Planform Design

Design of the aircraft planform was driven by several high level factors, primarily:

- Accommodation of optimal payload configuration

- Lift & drag characteristics at cruise and takeoff
- Manufacturing restrictions

In order to fit the payload specified by the score optimizer, the chord of the body airfoil was chosen to allow a tennis ball diameter to fit easily within the airfoil's maximum thickness (this can be seen in the profile view in Figure 3). This resulted in the primary Fauvel section having a chord of 571 mm. Wing loaded payload was also considered, but with the NACA24112 airfoil this would have required an unreasonably large wing chord. Since the wing airfoil has better performance than the body airfoil, we designed towards minimizing the spanwise width of the body section in favor of greater wing surface area. However, for optimal payload arrangement, we kept the width large enough to fit three tennis ball diameters, with some slight overlap into the transition section. The transition section itself was a linear taper from the body to wing airfoil over a distance of 50 mm. This was based on the definition of a BWB aircraft as provided by the course instructor.

An analysis of planform induced drag as a function of lift coefficient and aspect ratio indicated that induced drag could be reasonably minimized for an aspect ratio of around 5 (this plot is shown in Figure 25). This was used in combination with an estimate of required surface area to guide the evolution of the planform design.

Initial estimates of the full span of the aircraft and the minimum wing tip chord were then determined based on manufacturing restrictions for the planned construction process. These estimates, along with the body planform designed in the first step, served as the base planform input into XFLR5 for simulation purposes. The base planform had no wing sweep, dihedral or twist, but it included the payload arrangement and a basic mass distribution for stability purposes. The wing, just like the body was tapered to approximate an elliptical lift distribution (shown in Figure 12). Two fixed angle of attack analyses, one at 0° and another at 5°, and one fixed lift analysis were run in XFLR5 using the 3D panel method. The maximum lift coefficient before stall was extracted from the fixed lift analysis, while the fixed angle of attack analyses provided speed varying lift and drag coefficients.

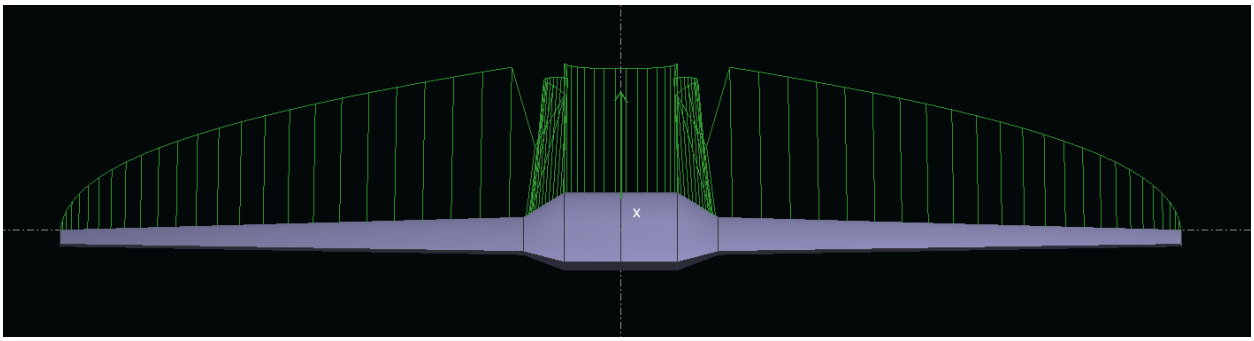

Figure 12 - Lift Distribution

Next, these results were input to the take-off distance calculations along with the calculated planform area, estimated total aircraft mass and a drag-minimizing aspect ratio (determined by examining where the induced drag VS aspect ratio curve begins to level off). The take-off script calculates the minimum planform area and corresponding semispan required to achieve the take-off bonus and whether or not the landing gear should be sloped with respect to the ground. The calculated

semispan replaced the planform semispan in XFLR5 and the process was repeated until the design converged with respect to semispan and maximum lift coefficient.

Finally, the wings of the converged planform were swept-back and dihedral and twist were added to obtain the desired moment, lift and drag performance. Sweeping the wings back caused the neutral point of the aircraft to move aft, increasing the static stability margin. Dihedral was added to improve the rolling stability of the aircraft, while washing out the wing tips also increased the zero-moment angle of attack. The iterative process was repeated until a suitable design converged, yielding the design as displayed in Figure 2.

2.3 Total Drag Estimation

A SolidWorks Flow Simulation was conducted to determine the total drag of the aircraft with the motor, landing gear, and wingtip fences installed. The simulation was run at a velocity of 15 m/s with a 0° α and a turbulence intensity of 10% to account for disturbances during the actual flight. Total drag force was predicted to be 1.7 N which results in a C_D of 0.0315 based on the planform area. Figure 13 illustrates the results of the CFD simulation, it also provides a visual verification of some trends noticed in XFLR5. For instance, XFLR predicts an upper surface transition at about 30% of the chord, a similar result of about 35% can be seen from SolidWorks, based on where surface shear stress reaches a maximum

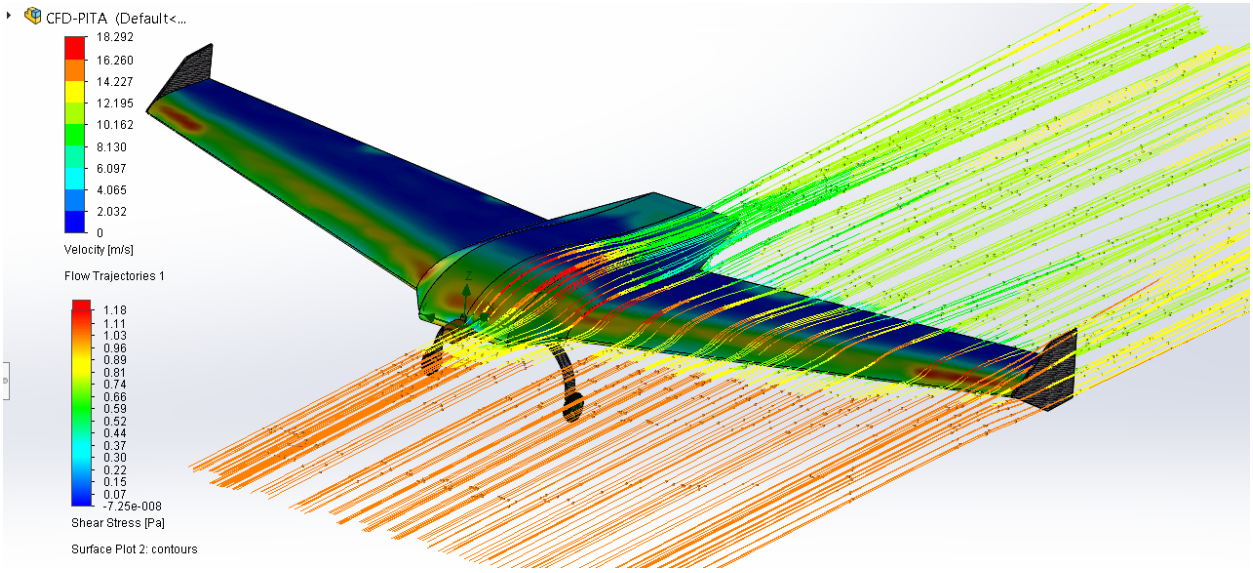

Figure 13 - SolidWorks CFD Simulation (Note Shear Stress Contours and Predicted Transition)

3 Stability & Control

3.1 Static Stability

For static stability, the planform was designed to keep the neutral point of the aircraft behind the center of gravity. This was primarily accomplished through front loading of the payload and high-mass components (battery, motor, etc.) along with swept back wings. The final parameters are:

- x_{CG} = 141 mm from body leading edge
- x_{NP} = 209 mm from body leading edge
- MAC = 324 mm
- Static margin = 21%

The center of gravity was estimated from CAD models, while XFLR5 provided the location of the neutral point. Note that the relatively high static margin gives ample safety factor for unaccounted components such as wires or fasteners that will be necessary in the final build.

3.2 Dynamic Stability

Dynamic stability of the aircraft was analyzed in XFLR5. A range of elevon deflection angles was specified, for which the program attempted to calculate the corresponding level flight condition. All dynamics stability analyses were performed on the wingtip fence version of the aerodynamic planform. Note also that XFLR5 runs only inviscid solutions when including control surface deflection calculations.

3.2.1 Longitudinal Modes

Both dynamic longitudinal modes are stable. The short period mode has a high damping ratio, which is good as it prevents drastic changes to angle of attack in steady flight. In comparison, the phugoid mode is very lightly damped; however, due to the low frequency, the period of oscillations will be long, so this will be easily correctable by pilot input. The information for each mode is summarized in Table 3, along with the root locus plot in Figure 14.

Table 3 - Longitudinal Modes Dynamic Stability

Mode	Natural Frequency (Hz)	Damped Frequency (Hz)	Damping Ratio	Stability
Short Period	5.46	4.694	0.594	Stable
Phugoid	0.137	0.137	0.012	Stable

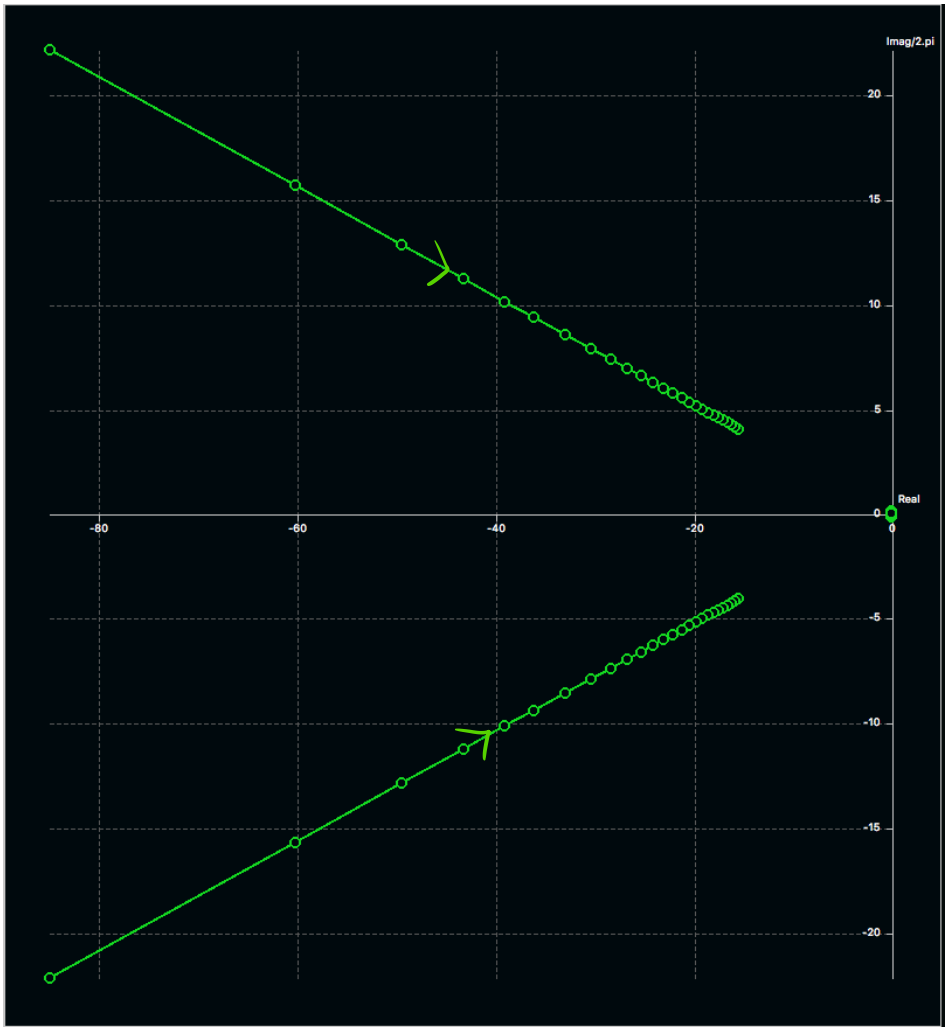

Figure 14 - Longitudinal Modes Root Locus Plot

3.2.2 Lateral Modes

The rolling mode is stable, with a very short half time, meaning any disturbances will quickly decay. The Dutch roll mode is only lightly damped; due to our specific BWB configuration this is difficult to avoid, given an intrinsic lack of vertical surface area. The spiral mode is unstable, but with a time to double of nearly two minutes, we do not anticipate this will have a significant detriment on the stability of the aircraft. Winglets were added to increase the stability of both the Dutch roll and spiral modes; wingtip fence area was increased until sufficient stability was achieved without much mass addition.

Table 4 - Lateral Modes Dynamic Stability

Mode	Info	Stability
Rolling	Time to halve: 0.014 s Time constant: 0.02	Stable

Dutch Roll	Natural frequency: 0.788 Hz Damped frequency: 0.787 Hz Damping ratio: 0.058	Stable
Spiral	Time to double: 115.5 s	Unstable

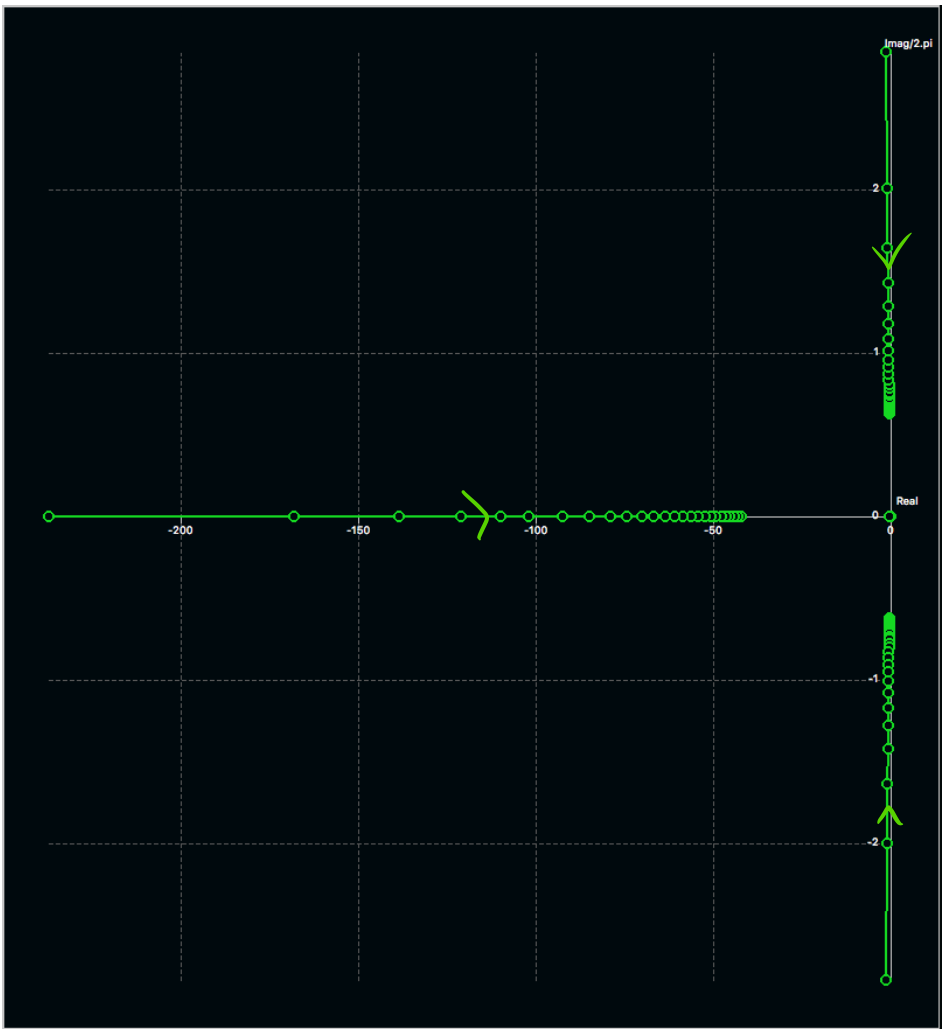

Figure 15 - Lateral Modes Root Locus Plot

3.3 Control Surface Design

Under the provided definition of a BWB configuration, the type of control surfaces available are elevons (combined aileron/elevator functionality) and a tail flap (pitch control and additional landing drag). Given that some functionality of the tail flap is also covered by the elevons, we would ideally want to achieve full controllability with only elevons in order to reduce actuation requirements and save weight. Therefore, the primary design choices made were:

- Elevon dimensions
- Inclusion of the tail flap

Elevons were sized in order to generate a minimum positive pitching moment at take-off. This ensures that the aircraft visibly lift off the runway within the required take-off distance. Analysis was done in XFLR5 on various control surface geometries over a range of deflection angles. Based on take-off distance calculations (see Section 6.2), these conditions are:

- 8.64 m/s velocity
- Minimum 5° AoA

The selected elevon geometry is shown in Figure 2. Hinge moment analysis was also done using XFLR5 software. The aircraft was placed in a "worst case" scenario of $\pm$ 30° deflection at 25 m/s, which corresponds to maximum control surface deflection in a steep dive. Under this loading case, the elevon experiences a hinge moment of 0.017 N·m. The stall torque of the servo is 0.1 N·m, a factor of 5.88 over the maximum loading case.

4 Structural Analysis

4.1 Material Selection

At this scale, RC aircraft are typically constructed using a rib and spar technique consisting of balsa wood and a Mylar wing covering. An alternative method consists of a using carbon fiber to fabricate a load bearing monocoque wing. Carbon fiber composite components have seen extensive use in the aerospace industry due to an extremely high strength to mass ratio. Upon completion of a trade study, it was concluded that a carbon fiber monocoque design would provide a number of advantages, which are stated below.

- High degree of similarity between CAD model and as-built aircraft: the aerodynamic model developed from XFLR5 can be converted into a SolidWorks CAD model, which in turn is translated to a surface mould (see Manufacturing section for more details). Having this one-to-one translation from design to fabrication ensures that no geometric details are lost and very few airframe compromises are introduced from the construction process. With a high fidelity fabricated model, the final aircraft performance will be much more similar to simulated results.
- Fine control over surface finish: Airfoil geometry can be accurately reproduced in the fabricated model and the surface finish can be finely controlled. This has the potential to increase laminar flow and airfoils will likely behave as in XFLR5.
- Durability for repeated flights: Due to the high strength to mass ratio of carbon, for the same aircraft mass as a rib and spar construction, a carbon fiber aircraft will have a significantly higher factor of safety. Over a number of loading cycles, the carbon aircraft is more likely to maintain its shape and develop little wear.
- Payload arrangement freedom: High stiffness values of carbon fiber allow for the wing spar to be removed and all loads to be transmitted through the monocoque shell. This not only saves weight but also permits a greater freedom to move the payload around, without having to arrange payload around a spar.

Although carbon fiber has many significant advantages, the major drawbacks are fabrication complexity and cost. To account for this increase in complexity and relative limited reference design at this RC scale, extensive structural calculations were conducted and a detailed fabrication plan has been

created (see the Manufacturing section). The high cost can be offset through careful material acquisition and purchasing in bulk.

4.2 Primary Reference Design

Figure 16 shows the primary reference design considered for the structural design of a carbon monocoque wing. This was designed by Brican Flight Systems, who produce carbon fiber based UAVs for aerial observation [5]. The outer surface composed of a gloss-coated plain-weave carbon fiber which bears a portion of the aerodynamic loads. Due to the large 5 m wing space and relatively short chord, the design includes a carbon sandwich panel spar to bear the majority of the load. Uni-directional carbon fiber cap strips can be seen at the top and bottom of this sandwich panel which serve to provide additional bending stiffness. In order to prevent shell buckling, a structural foam core with a fiberglass surface is bonded to the primary carbon surface. Since the production value of this wing segment is quite high, the design needed to be simplified to permit fabrication in a more reasonable time frame. For structural design of PITA Mk. CDVI, the starting case was taken to consist simply of one layer of carbon fiber conformed to desired shape of the wing bodies.

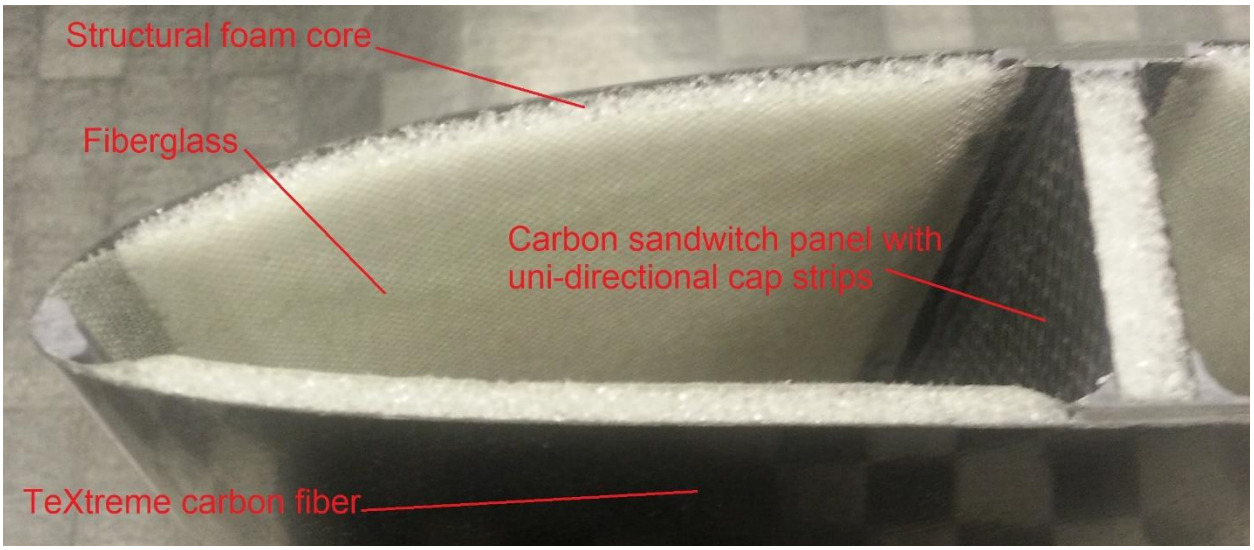

Figure 16 - Brican Carbon Fiber Wing Reference Design

4.3 Structural Design Methodology

Structural design followed an iterative approach, starting with base case as described above and adding more complex features (foam core, spar, ribs, etc.) each iteration if the desired load case was not met. SolidWorks FEA was selected as the an appropriate means to conduct the analysis as it provides a composite simulation feature where sandwich panel layers can easily be defined. In order to reduce the simulation time, only half of the aircraft structure was simulated, as the aerodynamic forces are assumed to be symmetric. The objectives of the FEA were selected as follows.

- Determine the specific number of layers of carbon fiber.
- Determine the type of carbon fiber to use (Cytec or TeXtreme) and thus the minimum layer thickness.
- Determine the necessity of a foam core and/or a spar.

Each design iteration was evaluated against the following criteria to determine if it was a valid solution:

- Minimize mass: assuming density values given in the material datasheets (see Appendix 7B), the total airframe structural mass shall be less than 500 g, as set during preliminary mass estimations.
- Factor of safety in yield: due to the potential errors introduced during fabrication, the minimum factor of safety should be at least 4.0 across all sandwich panel layers.
- Maximize buckling factor of safety: due to difficulties in predicting composite failure mechanisms such as delamination, core shear and microbuckling [6], the design should seek to have a high bucking factor of safety.
- Complexity: to facilitate reasonably rapid construction, designs that require unproven or highly advanced construction techniques should be avoided.

4.4 Structural FEA Setup

The SolidWorks surface model used for the simulation was translated directly from the final body shape in XFLR5. To reduce the simulation time and complexity, wingtip fences were excluded from the FEA. As seen in Figure 17, the center profile was rigidly fixed and a distributed force was applied over the entire lower surface of the aircraft. In order to simplify the analysis, it was assumed that the lift force would be evenly distributed over the wing instead of the elliptic lift distribution in XFLR5. To account for any limitations of this assumption, the lift force acting on the aircraft was calculated based on a maximum speed of 25 m/s achieved in a dive and the resulting C_L. Substituting the necessary values into Equation 1, the lift force over the half wing segment is calculated to be 71 N.

$$L_{half} = \frac{1}{4}\rho v^2 S C_{L,max}$$

Equation 1 - Lift Generated by Half of Wing-body

where ρ is assumed to be 1.225 kg/m^3, v is taken as the maximum dive speed of 25 m/s, S is the planform area of 0.392 m^2, and a $C_{L,max}$ of 0.946 taken at α = 12°.

With a total lift force over the entire aircraft of 142 N and using the mass stipulated in the mass budget, this results in a maximum load factor of n_{max} 10.9. It is important to note that this load factor is significantly higher that past AER406 designs, however, the design team believes that a high load factor is necessary to account for uncertainties in the performance of a carbon fiber monocoque design.

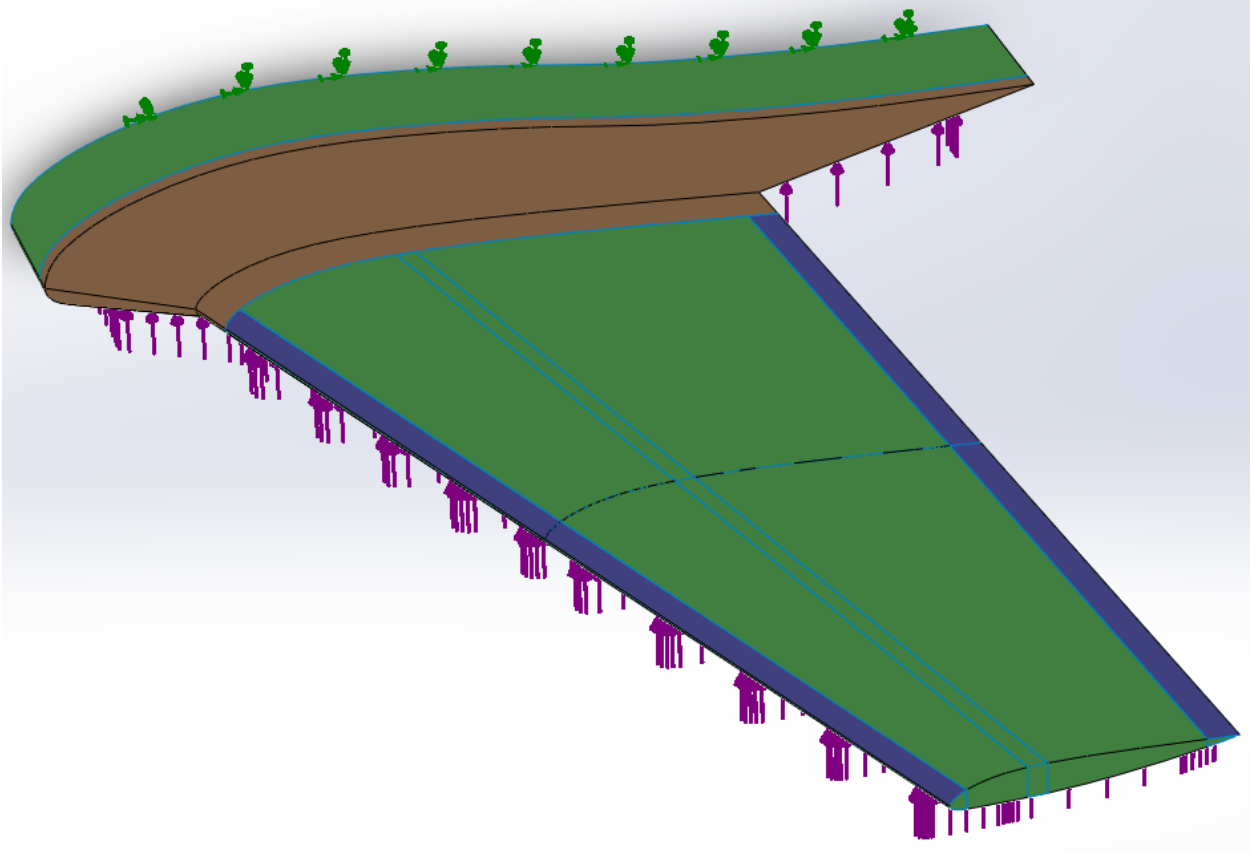

Figure 17 - Aircraft Structure FEA Setup and Surface Region Definition

4.5 Structural FEA Results

Over the first few iterations, it quickly became apparent that shell buckling was going to be a significant design driver since the carbon fiber layers are very thin. In order to avoid buckling the 2 mm foam core was added. To allow for the detailed control over the number of carbon fiber layers and usage of the foam core, the structure was divided into three separate regions as seen in Figure 17. Each region had a different number of layers to account for trends noticed in the FEA, Table 5 provides a summary of the final structure and reasoning.

Table 5 - Sandwich Panel Parameters According to Surface Region Definition

Region	**Color**	**Selected Layers ***	**Layer Thickness (mm) ***	**Fiber Orientation (relative to span)**	**Reasoning**
Lifting surfaces	Green	1 - TeXtreme 1 - Divinycell F50 1 - TeXtreme	0.1 2.0 0.1	-45° N/A 45°	Foam core added to solve wing buckling that typically occurred around mid-span.
Transition section between airfoils	Orange	1 – TeXtreme 1 - TeXtreme 1 - Divinycell F50 1 - TeXtreme	0.1 0.1 2.0 0.1	-45° 0° N/A 45°	Highest stress concentration occurred around leading edge of the transition section due to highly angled

					surfaces. Additional carbon added to raise global minimum FOS.
Leading and trailing edges	Purple	1 - TeXtreme 1 - TeXtreme 1 - TeXtreme	0.1 0.1 0.1	-45° 0° 45°	Foam does not conform well to high curvature and is too thick for trailing edge. Minor buckling tendencies removed by adding additional carbon layers

* Note: All layers listed from outer layer to inner layer

4.5.1 Factor of Safety Plot

Using the parameters stated in Table 5, Figure 18 shows the factor of safety plot, with respect to stress across all sandwich panel layers, over the entire aircraft. A minimum factor of safety of 7.3 is attained in the transition region between the two different airfoil profiles. Although, not present in the simulation geometry, a small radius fillet will be added to this transition section to further reduce the stress concentration. The structural failure mechanism was based on Tsai-Hill failure criterion [7], which takes into account the anisotropic behaviour of carbon depending on the fiber orientation. It is important to note that this failure mechanism does not consider delamination between layers, thus maintaining a higher FOS better accounts for any uncertainty.

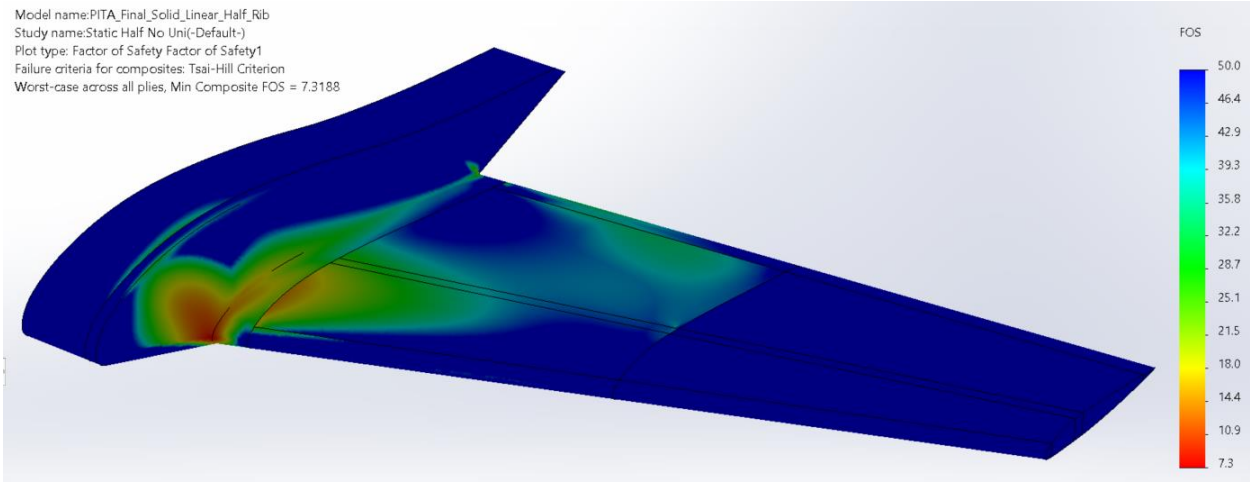

Figure 18 - SolidWorks Factor of Safety Plot at Maximum Load Factor

4.5.2 Buckling Mode Plot and Buckling Factor of Safety

SolidWorks predicts a buckling load factor of safety of -12.8, where the buckling load factor is a value that shows buckling trends. The further the BLF value is from zero, the less likely the design is to buckle. Figure 19 shows a control plot of the first buckling mode shape as predicted by SolidWorks. The green circular region represents where buckling is most likely to occur. Initial simulations predicted that buckling would occur closer to the mid-span of the wing and at much lower BLF. To correct for this tendency, a sandwich panel rib (same layer orientation as the wing) was added at the mid-span location. This shifted the location of buckling towards the center of the aircraft where the airframe was stiffer due to the additional layers of carbon used for the airfoil transition region.

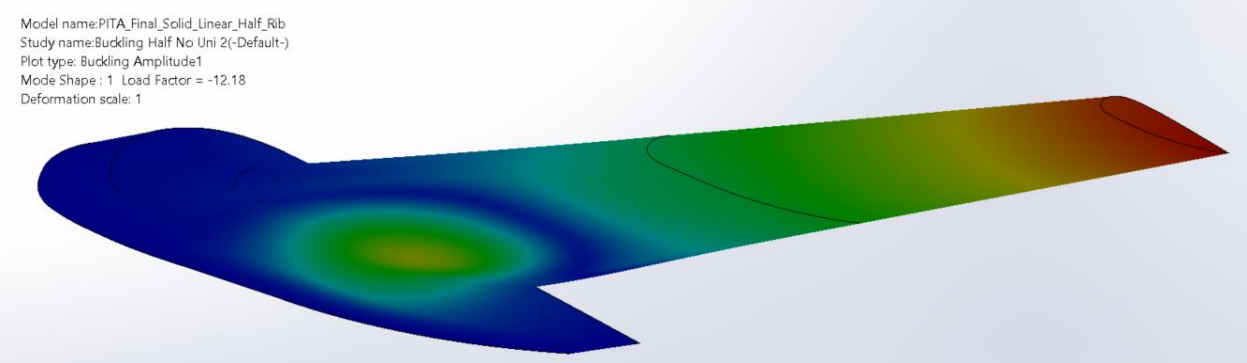

Figure 19 - SolidWorks Buckling Mode Shape Plot at Maximum Load Factor

5 Manufacturing

Due the complexity of manufacturing a composite aircraft and a limited availability of reference designs at this scale, the following fabrication section provides a detailed description of exactly how the design team intends to fabricate the PITA Mk. CDVI.

5.1.1 Carbon Fiber Mass Investigative Study

A trial composite manufacturing layup was conducted to determine the mass per unit area of various types of sandwich panels. Two types of carbon were tested: Cytec T300 plain weave with a thickness of 0.23 mm and TeXtreme 1000 with a thickness of 0.1 mm (material data sheets can be found in Appendix 7B). For the sandwich core, Divinycell F50 structural foam was used as it was the thinnest available (2 mm) and conformed well to curvature. A total of 8 different sandwich panels were fabricated with combinations of 2 to 6 layers for the different types of carbon fiber. After the epoxy had cured, each panel was cut to a measurable size and weighed. The complete list of layer combinations and results can be seen in Appendix 7C. It can be concluded from the investigation that it is critical to control the epoxy-to-carbon mass ratio to ensure sufficient layer adhesion without adding unnecessary epoxy mass. With an epoxy-to-carbon mass ratio of 0.7:1 it is possible to achieve an area density in the range of 480 g/m^2 to 520 g/m^2 using 2 layers of TeXtreme and the foam core. Since this sandwich panel has the lowest area density, it served as a benchmark for the aforementioned structural analysis.

5.2 Mould Design

Two options exist for creating a monocoque carbon part: a cavity mould were the carbon is placed into a precut part or an external mould where the carbon is wrapped around a precut part. A cavity mould is best suited for this design as surface finish and shape can be finely controlled to create an accurate aircraft body. The mould cavity will be cut from RenShape 440 Styling Board which is fast to machine and provides good surface definition. It is necessary to break the mould into a total of 4 different parts as shown in Figure 20. Having one continuous bottom mould allows for the wing twist and dihedral features to be easily aligned. Three separate top moulds permits placement of some internal components, such as wires and servos, before the top and bottom surfaces are bonded together. These moulds will be cut using a ShopBot 3-axis CNC mill using Surfcam 2014 to create the toolpaths. Figure 21 shows the final exported SurfCam toolpath before it was cut on the CNC mill. Initial predictions show total CNC mill time of approximately 20 hours (note that the CNC will run unsupervised to parallelize work). Before the moulds can be used to create the carbon parts, the surface must be sanded, sealed, and release-coated, as this is necessary to produce the desired smooth surface finish.

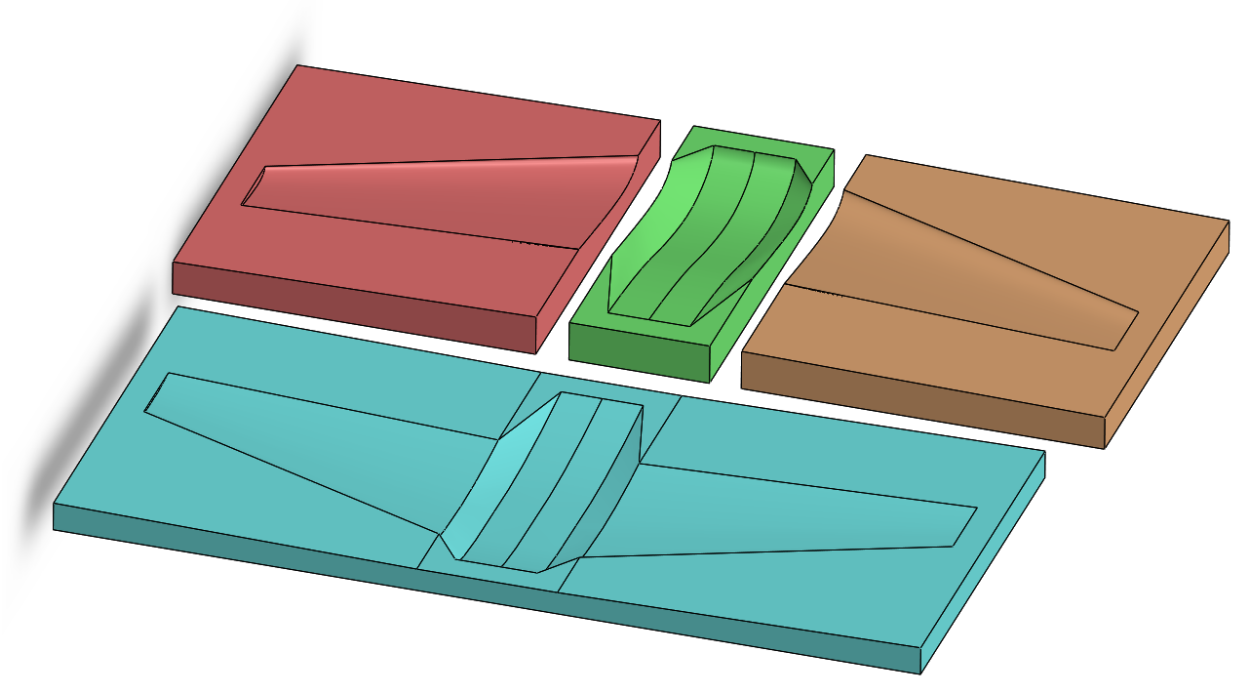

Figure 20 - Four-Part Cavity Mould Layout

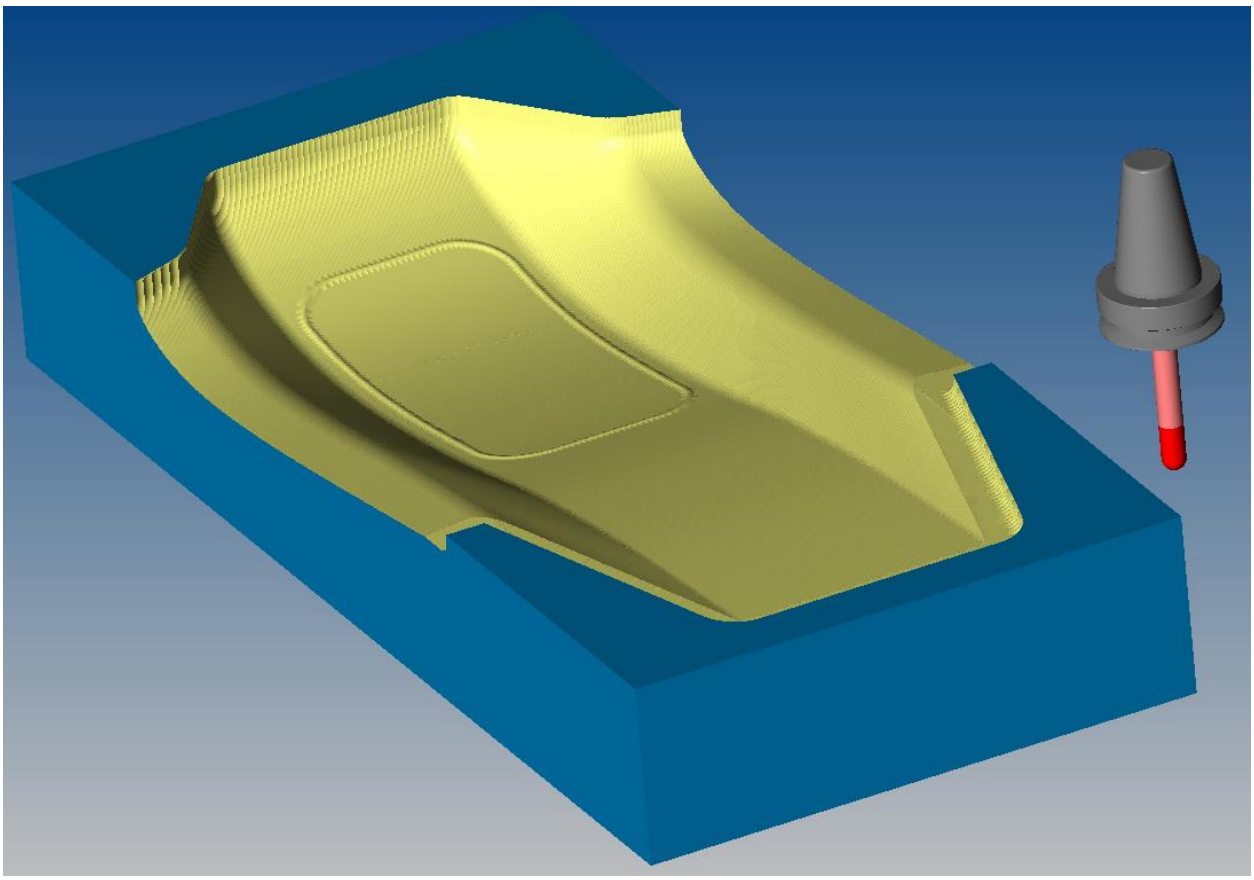

Figure 21 - SurfCam Generated Toolpath for Top Center Body Section (Note: Alignment Feature for Access Hatch)

5.3 Layup Process

Material data sheets for the carbon fiber, foam core, and epoxy can be found in Appendix 7B. The basic fabrication process for the composite parts will consists of the following steps:

1. Carbon will be cut into the necessary patterns for each mould. During the layup process epoxy is manually infused into carbon fiber fabric and excess epoxy is removed. The wet-up carbon pieces are placed into the mould according to Table 5. Each mould layup will take at most 2 hours to complete.
2. Once all carbon and foam pieces are placed, the entire mould is placed into a bag and sealed. A vacuum pump draws out all the air, using the atmospheric pressure to compress all layers into the mould cavity. The entire part will be heated to ensure the epoxy cures at a reasonable rate in approximately 8-14 hours.
3. All carbon components will be removed from the vacuum bag and trimmed to the desired shape.
4. Upon placement of the necessary internal components, the three upper surface segments will be bonded to lower surface segment using a bead of epoxy running the length of the LE and TE. Two strips of carbon fiber will be placed at each seam to ensure a rigid connection between each segment.

5.4 Secondary Structure Fabrication

A number of components will need to be fabricated separately from the main carbon structure and attached later in the construction process.

5.4.1 Access Hatch

As seen in Figure 21, a feature has been added to the mould to mark the position of the access hatch to be cut out, it will consist of the same number of layers as the main wing body. To ensure a rigid connection between the hatch and top wing surface, additional layers of carbon fiber will be placed around the perimeter of the hatch outline to create a lap-joint. The hatch will then be bolted to the aircraft body using at least four bolts, similarly to the carbon *Hyperion* BWB aircraft [8]. Any gaps or protrusions will be sealed using wax to promote laminar flow.

5.4.2 Control Surfaces

The monocoque carbon structure makes it possible to implement “concealed” actuation methods such as the example seen in Figure 22.

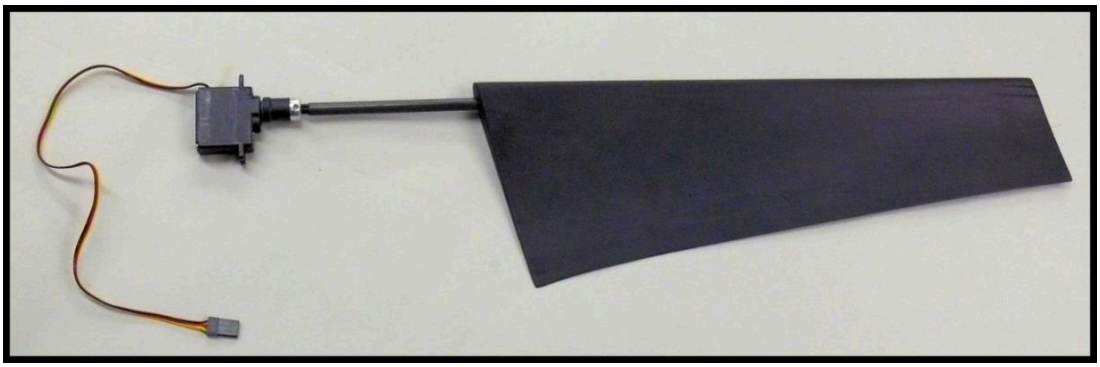

Figure 22 - Direct Servo Actuation [9]

This configuration is ideal because it eliminates any exterior components protruding through the airframe, reducing drag. From Section 3.3, we know that our servos have more than enough torque to handle the hinge moments directly. The only drawback is that this method may require customized servo attachments to the frame, potentially making the manufacturing process more complicated. Should this method prove impractical within the time constraints of the course, we can easily switch to a more conventional method of control horn/pushrod linkages.

6 Performance

The table below summarizes the performance and design of the aircraft. Any performance parameters obtained using XFLR5 employed a planform without wingtip fences as the inclusion of such devices introduced unnecessary errors in the simulations. The following sections describe the calculations and assumptions made to determine any parameters not discussed previously.

Table 6 - Aircraft Design & Performance Summary

Aircraft Parameter or Performance Metric	Value
b (m)	1.38
S (m^2)	0.392
AR	4.86
EW (kg)	0.840
m (kg)	1.324
Payload Configuration	8 tennis, 5 ping pong, 0 golf balls (487 g)
$C_{L,max}$	0.852
α_{stall} (°)	12
Static Margin (%)	21
v_{cruise} (m/s)	15
α_{trim} (°)	5.36
$\delta_{e,trim}$ (°; > 0 => downward)	-13.75
$C_{L,trim}$	0.236
$C_{D,cruise}$	0.023
$(C_L/C_D)_{cruise}$	10.3
T_{cruise} (N)	4.1 (max throttle)
$(T/W)_{cruise}$	0.316
ϕ (°)	70
r_c (m)	8.35
ω_c (rad/s)	1.80
t (s; 3 laps)	36.74 (using level turns)
s_g (m)	4.28
α_g (°)	5
Estimated Score (excluding PPB)	1,710

6.1 Propulsion

One of the most constraining aspects of the design is the propulsion system. Since the motor and power supply are provided, only the propeller can change the characteristics of the power plant. In general, a larger propeller will generate higher thrust at the same speeds as a smaller diameter

propeller, while increasing propeller pitch allows a propeller to operate at higher speeds than with a lower pitch. Large diameter, low pitch propellers therefore offer rapid acceleration and are well suited for take-off. Smaller, higher pitch propellers enable high-speed performance and efficiency. As such, the three primary propellers, 8×8, 9×6 and 10×5, were compared using MotoCalc to determine which one is best suited for the design at hand. From this analysis, the 9×6 propeller was selected to enable high-speed flight while providing reasonable take-off distances. The thrust and propeller RPM versus airspeed graph for the selected propeller is displayed below.

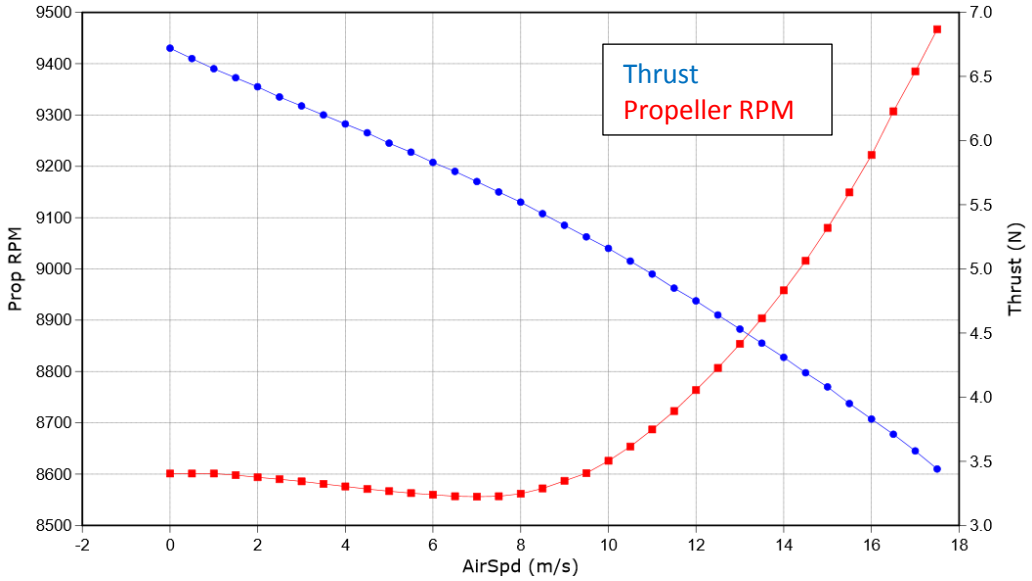

Figure 23 - 9×6 Thrust & Propeller RPM VS Airspeed

Based on the data in Figure 23 and the drag calculated using CFD for the full aircraft, including landing gear and other external features, indicates that the maximum possible flight speed ignoring trim drag effects is roughly 20 m/s.

As can be seen in Figure 1, the propeller is in a puller or tractor configuration. The tractor configuration was chosen to minimize the mass of the overall propeller assembly and the landing gear length while also offering simpler structural connections. In addition, the tractor configuration has a beneficial effect on pitch stability, as it tends to shift the CG towards the nose of the aircraft, and helps the flow over the body stay attached at low speeds by forcing turbulent flow.

6.2 Take-off Distance

The take-off distance was calculated as the length of the ground roll for a take-off maneuver, as advised by Prof. Grant. The ground roll length was determined by numerically integrating the equation

$$s_g = \int_{v_{hw}}^{v_{LO}} \frac{m(v - v_{hw})}{T - D - \mu_r(mg - L)} dv$$

Equation 2 - Ground Roll Integral

where μ_r was estimated to be 0.08, v_{LO} was taken as 10% greater than the stall speed and v_{hw} was assumed to be 3 m/s. The stall speed is the speed where level flight occurs with the maximum possible C_L, $C_{L,max}$, which is approximately 7.90 m/s, corresponding to a total mass of 1.3 kg and $C_{L,max}$ = 0.852. To

provide a conservative estimate, the thrust was interpolated linearly between the minimum and maximum thrust values (and the corresponding airspeeds) obtained from MotoCalc. Using the C_L and C_D versus speed data obtained from XFLR5, including ground effects, the lift and drag employed spline interpolants for their respective coefficients during the integration. The lift coefficient was calculated at an angle of attack of 5° due to landing gear slope to reduce take-off distance as compared to that without an angle of incidence.

6.3 Cruise & Trimming Conditions

The trimming calculations were performed for three different cruise speeds to provide options for the flight plan. The values for $C_{L\delta}$ and $C_{M\delta}$ were obtained by linear approximation from results in XFLR5 yielding 0.590 rad^{-1} and -0.298 rad^{-1} respectively. Also based on results from XFLR5, C_{M0} was determined to be 0.005. The trimmed angle of attack and elevon deflection angle were calculated from

$$\begin{cases} \alpha_{trim} = \dfrac{C_{M\delta}C_{L,trim} + C_{M0}C_{L\delta}}{det\ C} \\ \delta_{e,trim} = -\dfrac{C_{M\alpha}C_{L,trim} + C_{M0}C_{L\alpha}}{det\ C} \end{cases}, \quad C \coloneqq \begin{bmatrix} C_{L\alpha} & C_{L\delta} \\ C_{M\alpha} & C_{M\delta} \end{bmatrix} = \begin{bmatrix} 4.04 & 0.590 \\ -0.819 & -0.298 \end{bmatrix} rad^{-1}.$$

Equation 3 – Trimmed AoA & Elevon Deflection

Table 7 below summarizes the trim and cruise conditions for the three different cruise speeds. Note that C_D values include parasite drag of landing gear and external components calculated using CFD.

Table 7 - Trim & Cruise Conditions

v_{cruise} (m/s)	15	18	20
$C_{L,trim}$	0.236	0.164	0.133
$C_{D,cruise}$	0.023	0.016	0.014
α_{trim} (°)	5.36	3.65	2.92
$\delta_{e,trim}$ (°)	-13.75	-9.05	-7.05

6.4 Maneuvering Performance

Before choosing a particular bank angle and calculating the corresponding course flight time, it is critical to determine the maneuvering envelope of the aircraft. The maneuvering envelope is shown in

below. The point indicated in the figure is near to the designed flight conditions and provides the stall limit for a level turn. The following discussion provides the actual designed values.

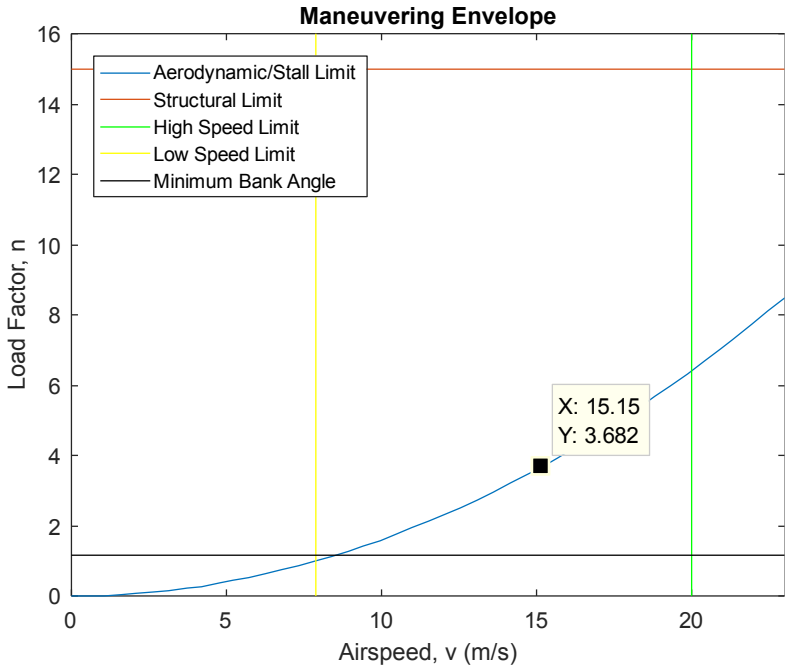

Figure 24 - Maneuvering Envelope

In , the low speed limit corresponds to the stall speed of the aircraft (≈ 7.90 m/s). The minimum bank angle line indicates the load factor of a level turn while banked at the minimum angle, 30°. The high speed limit occurs at the condition when thrust equals drag at maximum throttle. In other words, this indicates the maximum speed that maintains level flight. The aerodynamic limit represents the maximum possible load factor that the aircraft can support without stalling the wing. The load factor indicated for the near-design flight condition (3.682) yields a stalled bank angle of approximately 74°. The structural limit is shown only for completeness because its actual value is significantly higher and therefore irrelevant, since the high speed and aerodynamic limits intersect beneath it. This means that for any level flight maneuver, the resulting load factor cannot cause structural damage.

Based on the maneuvering envelope, a bank angle of 70°, with turning airspeed equal to the cruise airspeed, was taken to estimate flight time for three laps of the course. The turn radius and rate for a level turn at the selected bank angle were calculated as

$$r_c = \frac{v^2}{g \tan \phi} = 8.35\ m, \quad \omega_c = \frac{v}{r_c} = 1.80\ rad/s.$$

Equation 4 - Level Turn Radius and Rate

These values yield a flight time of 36.74 s and a flight time score bonus of 1.27. It is intended to use hammerhead turns to reduce further the flight time and this advanced maneuver is within the capabilities of our test pilot.

7 Scheduling

Project Planner

Period: 11

Plan Duration | % Complete
Actual Start | Actual (beyond plan)
% Complete (beyond plan)

Select a period to highlight at right. A legend describing the charting follows. Yellow fill in the week # indicates a de

ACTIVITY	PLAN START	PLAN DURATION	ACTUAL START	ACTUAL DURATION	PERCENT COMPLETE
Scheduling	1	2	2	1	100%
Score Optimization	2	3	2	3	100%
Propulsion Design	3	1	3	2	100%
Configuration Selection	3	1	3	2	100%
Propeller Selection	3	1	3	1	100%
Aerodynamic Design	4	4	3	4	75%
Airfoil Selection	4	1	3	2	100%
Wing/Planform Geometry	4	4	3	3	100%
Payload Bay Sizing/Arrangement	6	1	3	2	100%
Final Design Validation	8	1	8	1	0%
Stability & Control Design	6	1	4	5	25%
Static Stability Analysis	6	1	4	2	75%
Control Surfaces	6	1	6	2	0%
Dynamic Stability Analysis	6	1	6	3	0%
Structural Design	4	5	4	5	28%
Material Selection	4	1	4	1	100%
Airframe Design	5	3	6	3	0%
Secondary Structure Design (Landing Gear & Fairings)	7	2	7	2	0%
Load/Failure Analysis	8	1	5	4	10%
Electrical	9	1	9	1	0%
Wiring Layout	9	1	9	1	0%
Component Layout	9	1	9	1	0%
Manufacturing	4	8	6	6	0%
Material Acquisition	4	4	6	4	0%
Mold/Jig Preparation	8	1	8	1	0%
Component Fabrication	9	2	9	2	0%
Primary Body	9	2	9	2	0%
Secondary Components	10	1	10	1	0%
Assembly & Wiring	11	1	11	1	0%
Testing	12	1	12	1	0%
Control Check	12	1	12	1	0%
Zipline Test	12	1	12	1	0%
Flight Test	12	1	12	1	0%

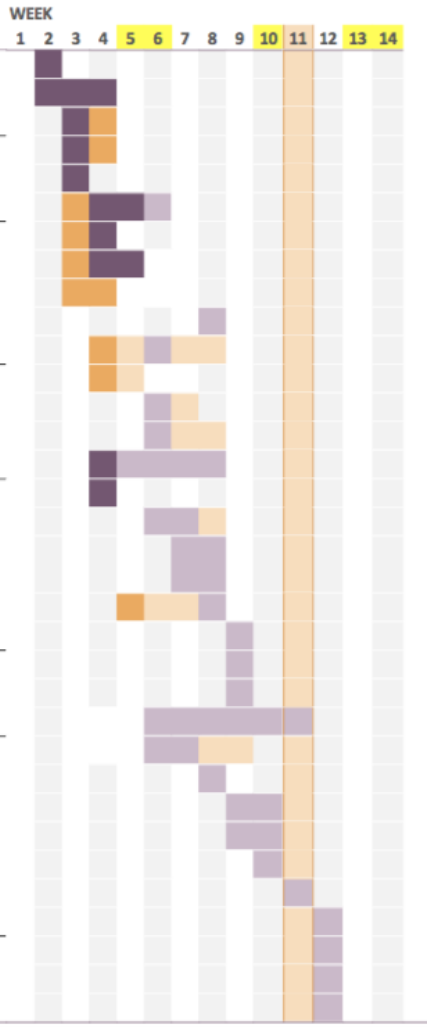

References

[1] M. Sargeant, T. Hynes, W. Graham, J. Hileman, M. Drela and Z. Spakovszky, "Stability of Hybrid-Wing–Body-Type Aircraft with Centerbody Leading-Edge Carving," *Journal of Aircraft,* vol. 47, no. 3, pp. 970-976, 2010.

[2] T. Ikeda, "Aerodynamic Analysis of a Blended-Wing-Body Aircraft Configuration," RMIT University, 2006.

[3] R. Liebeck, "Design of the BlendedWing Body Subsonic Transport," *Journal of Aircraft,* vol. 41, no. 1, pp. 10-25, 2004.

[4] "Airfoil Tools," 2017. [Online]. Available: http://airfoiltools.com/. [Accessed 15 January 2017].

[5] Brican Flight Systems, "TD100 UAV," Brican Flight Systems, [Online]. Available: http://bricanflightsystems.com/services/uav-configuration/. [Accessed 23 January 2017].

[6] C. Steeves, *Lecture Notes AER373: Solid and Structural Mechanics,* Toronto, 2015.

[7] Dassault Systemes, "Tsai-Hill Failure Criterion," SolidWorks, [Online]. Available: http://help.solidworks.com/2016/english/SolidWorks/cworks/c_Tsai-Hill_Failure_Criterion.htm.

[8] J. Koster, K. Uhmeyer and G. Soin, "Designing a Blended Wing Body Aircraft Globally," in *International CDIO Conference*, Cambridge, Massachusetts, 2013.

[9] AMRC Boeing, "Rapid Manufacturind Fixed Wing Powered UAV," AMRC Boeing.

[10] HPVDT, "Human Powered Vehicle Design Team (U of T)," 2015. [Online]. Available: http://hpvdt.skule.ca/.

[11] MatWeb, "Material Property Data," Matweb, 2017. [Online]. Available: http://www.matweb.com/index.aspx.

[12] "TeXtreme 1000," [Online]. Available: http://compositeenvisions.com/textreme-1000-hs-100gsm-2-95oz-spread-tow-carbon-fiber-1122.html.

[13] "Thornel T300," [Online]. Available: https://www.cytec.com/sites/default/files/datasheets/THORNEL_T300_052112.pdf.

[14] "Divinycell F50," [Online]. Available: http://www.diabgroup.com/Products-and-services/Core-Material/Divinycell-F.

[15] "Resin Formulators," [Online]. Available: https://www.evroberts.com/home/.

Appendices

A Induced Drag Calculation

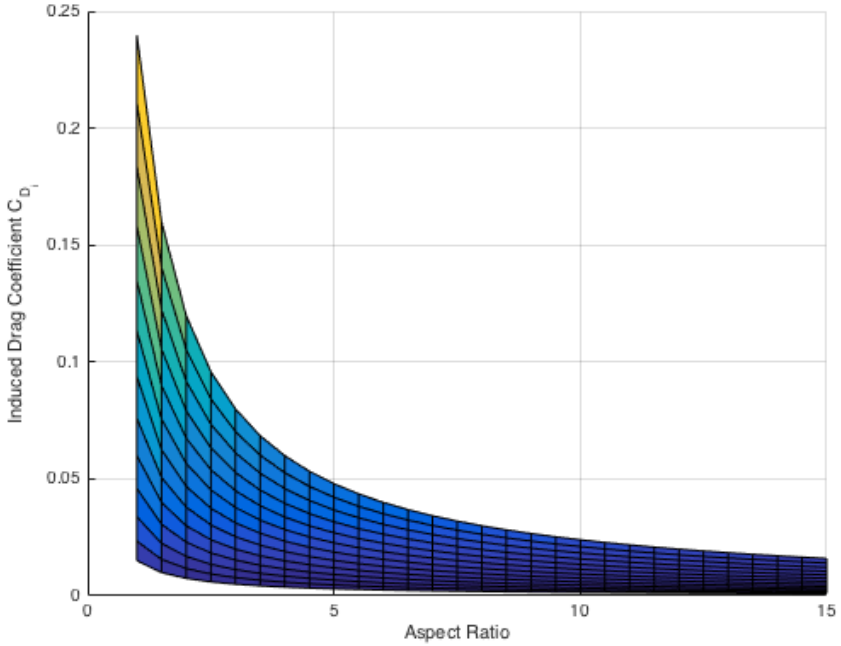

Figure 25 - Induced Drag VS Aspect Ratio (C_L = 0.2 to 1.0)

B Material Properties

Material properties are taken from the HPVDT material database [10] based on values obtained from the MatWeb online database [11].

Property	Woven Carbon Fiber	Divinycell F50 Core Material	Bonding Expoy
Elastic Modulus (MPa)	70,000	35	827.3
Poisson's Ratio	0.2	0.25	0.394
Shear Modulus (Mpa)	5,000	24	318.9
Tensile Strength (Mpa)	600	2.8	49.64225
Compressive Strength (Mpa)	580	1.2	98.595029
Yield Strength (Mpa)	580	1.2	N/A
Density (kg/m^3)	1,600	90	1,510

Datasheets for each of the materials can be found through the following links:

- TeXtreme 1000 [12]
- Thornel T300 3K [13]
- Divinycell F50 [14]
- Resin Formulators Epoxy Kit (RF 619 Hardener – RF 1366 Mod 3 Resin) [15]

C Carbon Samples Test Data

Sample	Layers	Length (mm)	Width (mm)	Thickness (mm)	Mass (g)	Area Density (g/m^2)	Est. Epoxy Mass (g)	Epoxy Ratio		Resulting Area Density (g/m	Aircraft Mass (g)
1,1	2	48.1	47.9	2.7	2.2	955	0.99	1.13		756	1481
2,1	3	49.65	47.95	2.74	3	1260	1.30	0.96		1079	1744
3,1	4	49	48.5	3.06	3.6	1515	1.45	0.80		1402	2007
2,2	4	48.4	48.2	3	3.6	1543	1.49	0.84		1402	2007
3,2	5	49.62	50.3	3.2	4.6	1843	1.87	0.79		1725	2270
3,3	6	50.45	52.14	3.5	5.7	2167	2.32	0.77		2048	2534
1,1T	2	50.19	48.275	2.45	1.9	784	0.97	1.68		516	1286
2,2T	4	48.7	48.25	2.61	2.2	936	0.74	0.66		923	1617
								Above is epoxy divided by carbon mass.			
Material Properties:								**Aircraft Info:**			
Carbon Fibre		647.7	65	0.23	8	190		Surface Area (m^2)	0.81445		
TeXtreme		78	118	0.1	1.1	120		Payload Mass (g)	487		
Sample Foam Core		610	96.5	2.2	8.5	144		Component Mass (g)	378.4		
DivinyCell F50 (mea		609.6	2438.4	N/A	186.1	125		Minimum Epoxy Ratio	0.7		
" (data sheet)		N/A	N/A	2.2	N/A	110					

D Calculation of Total Aircraft Structural Mass

Parameter	**Value**	**Unit**		
Cytek Carbon	0.16	kg/m^2	(0.19) measured	
Textreme	0.1	kg/m^2	(0.12) measured	
Divinycell F50	0.1	kg/m^2	(0.125) measured	
Epxoy-carbon ratio	0.7		(0.6) optimal	
epoxy-hardner	1345.6	kg/m^3		
Textreme-epoxy	0.17	kg/m^2		
cytek-epoxy	0.272	kg/m^2		
1-core-1 tek	0.44	kg/m^2	(0.492) measured	
2-core-1 tek	0.7	kg/m^2		
2-core-2 tek	0.78	kg/m^2	(0.875) measured	
Area Fractions (For Half)			**Mass (kg)**	**Notes**
Total SA	814481.93	mm^2		
	0.81448193	m^2	0.358372049	
LE-TE SA (Purple)	32104	mm^2		
	0.032104	m^2	0.02183072	3 tek
WING SA (Green)	302661	mm^2		
	0.302661	m^2	0.13317084	1-c-1
TRANSITION SA (Orange)	78685	mm^2		
	0.078685	m^2	0.0550795	2-c-1
FRACTION TOTAL			0.42016212	
FOS	1.1			
TOTAL /W MARGIN			0.462178332	

Note: That surface area (SA) fractions are determined from SolidWorks and layer mass uses parameters defined in Table 5.